Knee Surg Sports Traumatol Arthrosc
DOI 10.1007/s00167-014-3399-1

ANKLE

Magnetic resonance imaging characterization of individual ankle syndesmosis structures in asymptomatic and surgically treated cohorts

Thomas O. Clanton · Charles P. Ho · Brady T. Williams · Rachel K. Surowiec · Coley C. Gatlin · C. Thomas Haytmanek · Robert F. LaPrade

Received: 9 June 2014 / Accepted: 20 October 2014

Abstract
Purpose Historically, syndesmosis injuries have been underdiagnosed. The purpose of this study was to characterize the 3.0-T MRI presentations of the distal tibiofibular syndesmosis and its individual structures in both asymptomatic and injured cohorts.
Methods Ten age-matched asymptomatic volunteers were imaged to characterize the asymptomatic syndesmotic anatomy. A series of 21 consecutive patients with a pre-operative 3.0-T ankle MRI and subsequent arthroscopic evaluation for suspected syndesmotic injury were reviewed and analysed. Prospectively collected pre-operative MRI findings were correlated with arthroscopy to assess diagnostic accuracy [sensitivity, specificity, positive predictive value (PPV), and negative predictive value (NPV)].
Results Pathology diagnosed on pre-operative MRI correlated strongly with arthroscopic findings. Syndesmotic ligament disruption was prospectively diagnosed on MRI with excellent sensitivity, specificity, PPV, NPV, and accuracy: anterior inferior tibiofibular ligament (87.5, 100, 100, 71.4, 90.5 %); posterior inferior tibiofibular ligament (N/A, 95.2, 0.0, 100, 95.2 %); and interosseous tibiofibular ligament (66.7, 86.7, 66.7, 86.7, 81.0 %).
Conclusions Pre-operative 3.0-T MRI demonstrated excellent accuracy in the diagnosis of syndesmotic ligament tears and allowed for the visualization of relevant individual syndesmosis structures. Using a standard clinical ankle MRI protocol at 3.0-T, associated ligament injuries could be readily identified. Clinical implementation of optimal high-field MRI sequences in a standard clinical ankle MRI exam can aid in the diagnosis of syndesmotic injuries, augment pre-operative planning, and facilitate anatomic repair by providing additional details regarding the integrity of individual syndesmotic structures not discernible through physical examination and radiographic assessments.
Level of evidence II.

Keywords Syndesmosis ligament tears · Anatomy · Magnetic resonance imaging (MRI) · Arthroscopy · Diagnostics (sensitivity, specificity, NPV, PPV)

T. O. Clanton · C. P. Ho (✉) · B. T. Williams · R. K. Surowiec · C. C. Gatlin · C. T. Haytmanek · R. F. LaPrade
Departments of BioMedical Engineering and Imaging Research, Steadman Philippon Research Institute, 181 W. Meadow Drive, Suite 1000, Vail, CO 81657, USA
e-mail: charles.ho@sprivail.org

T. O. Clanton · C. P. Ho · C. C. Gatlin · C. T. Haytmanek · R. F. LaPrade
The Steadman Clinic, Vail, CO, USA

Introduction

The stability of the distal tibiofibular syndesmosis is conferred by the bony congruencies of the distal tibia and fibula and the ligaments of the syndesmosis including the anterior inferior tibiofibular ligament (AITFL), posterior inferior tibiofibular ligament (PITFL), and interosseous tibiofibular ligament (ITFL). Injuries to the distal tibiofibular ligaments are less common than lateral ankle sprains; however, the post-injury recovery time has been reported to be up to four times longer [7, 11, 19–21, 36]. If not accurately diagnosed and properly managed, these injuries may lead to post-traumatic arthritic changes and chondral defects over time [30, 31, 46].

In clinical practice, the diagnosis of a syndesmosis injury has centered around the injury mechanism, thorough physical examination, and standard radiographic findings

Published online: 15 November 2014

[including weight bearing views in the anteroposterior (AP), mortise, and lateral projections, when tolerated] [20]. Physical examination sensitivity rarely exceeds 50 %, often falling below 30 % in the general population [8, 13, 35, 37]. Heightened awareness has improved detection in the elite athlete; however, data still suggest insufficient sensitivity [21, 34, 45]. Furthermore, physical examination can be inconclusive, limited by pain, or entirely unfeasible in the presence of a concurrent distal fibular fracture [8, 35, 37]. Radiographic evaluation can be equally inconclusive as standard and stress radiographic measurements are variable and are significantly influenced by extremity rotation [4, 14, 23, 26, 29, 33, 38, 39, 41]. As a consequence of insufficiently sensitive diagnostic techniques, syndesmotic injuries have been frequently underdiagnosed by current clinical modalities [4, 5, 8, 13, 16, 23, 24, 26, 29, 33–35, 37, 42, 44].

More recently, high-field magnetic resonance imaging (MRI), particularly at 3.0-T, has improved ankle and syndesmosis imaging compared with imaging at 1.5-T [2, 12]. The majority of current literature has evaluated the MRI appearance of the syndesmosis in patient populations and cadaveric models at lower field strengths [6, 8, 13, 15–18, 22, 25, 27, 34, 39, 43]. Therefore, the purpose of this study was to comprehensively characterize the MRI presentation of the structures of the distal tibiofibular syndesmosis in both asymptomatic volunteers and an injured patient cohort with the goal of evaluating and improving diagnostic sensitivity and reliability of 3.0-T MRI. Additionally, the authors sought to compare the diagnostic accuracy of 3.0-T MRI in evaluating the syndesmotic ligaments (AITFL, PITFL, ITFL), synovial recess, and tibiotalar articular surfaces, compared to the gold standard of ankle arthroscopy. This was performed in order to assess the ability of MRI to accurately and reproducibly visualize individual syndesmotic structures and diagnose clinically relevant injuries.

Materials and methods

Between January 2010 and November 2013, 21 consecutive patients (5 female and 16 male) with a mean age of 35 years (range 16–60 years) who underwent arthroscopically assisted surgery for ankle pathology and suspected syndesmotic injury by a single senior foot and ankle fellowship trained orthopaedic surgeon (TOC) were included in the study. Patients with a suspected syndesmosis injury based on the findings of physical examination, patient history, and standard radiographs were identified for initial inclusion. Of these patients, those with a pre-operative standard MRI at 3.0-T read by a single senior musculoskeletal radiologist (CPH) and subsequent ankle arthroscopy performed by a single senior foot and ankle fellowship trained orthopaedic surgeon (TOC) were included in the final analysis. All patients had a pre-operative MRI within 2 months of arthroscopic surgery, except for one patient who had an MRI 4 months pre-operatively. No patients meeting the criteria for inclusion had previous ankle surgery requiring hardware implantation; therefore, a standardized scanning protocol could be implemented and interpreted without significant metal-induced artifact for all included patients. Detailed pre-operative patient parameters including the mechanism of injury, findings of the physical and radiologic examination, and surgical indications can be found in Table 1.

For evaluation of the normal anatomy of the syndesmosis, ten asymptomatic volunteers were prospectively enrolled in the study. In order to parallel the included patient population, sampled volunteers were between the ages of 18–62 and distributed equally among three cohorts (18–32, 33–47, and 48–62). Volunteers were deemed asymptomatic by a self-administered subjective scoring form [the Foot and Ankle Ability Measure (FAAM), Foot and Ankle Disability Index (FADI), and the Tegner activity scale in addition to pain/swelling/stiffness/visual analogue score], an objective clinical examination performed by a foot and ankle fellowship trained orthopaedic surgeon (TOC), and an MRI examination which was evaluated by a senior musculoskeletal radiologist (CPH).

Magnetic resonance imaging

Following a thorough pre-operative physical examination, all patients underwent pre-operative MR imaging at 3.0-T (Verio, Siemens Medical Solutions, Erlangen, Germany) using an eight-channel dedicated foot and ankle coil (Invivo, Gainesville, FL, USA). Asymptomatic volunteers underwent an identical protocol. Both patients and volunteers were positioned supine for the MR examination. Details of the scanning protocol can be found in Table 2.

Magnetic resonance imaging examination findings including ligament tearing/sprain/scarring, tendon status and pathology, syndesmosis status including diastasis and synovitis, effusion, and chondral injury were prospectively recorded pre-operatively and blinded to the results of subsequent arthroscopy. The criteria for diagnosing ligament tears included ligament discontinuity and/or non-visualization of the ligament at the level of the tibial plafond. When either or both of these criteria were observed on one or more of the MR sequences, the injury was diagnosed as a ligament disruption (tear). Ligament sprains and scarring presented with irregular margins, increased intermediate to high signal, and/or elongated ligament contour on MRI. All asymptomatic volunteer scans were evaluated using the same criteria in order to detect any signs of sub-clinical

Table 1 Patient demographics, injury mechanism, indications for surgery, and clinical findings

M/F	Age	Injury mechanism	Acute/chronic	Indication(s) for surgery	Physical exam						Radiographs
					P/T	CT	ER	SQ	AD	TT	
F	16	Ankle sprain; volleyball	Acute	Severe high ankle sprain; pain	+	−	±	N/A	−	−	Unremarkable
M	51	Snowboarding	Acute	Maisonneuve fracture; syndesmosis tear (MRI)	+	−	+	+	−	−	Spiral fracture, proximal fibula
M	53	No specific injury	Chronic	Anterolateral ankle pain, 5+ years; syndesmosis scarring (MRI)	+	N/A	−	N/A	−	−	Unremarkable
F	60	Chronic ankle sprains	Chronic	Chronic ankle sprains; peroneus brevis tear (MRI)	+	N/A	N/A	N/A	−	−	Unremarkable
M	25	External rotation injury; football	Acute	Syndesmosis injury (physical exam, radiologic findings)	+	−	+	N/A	−	−	Unremarkable
M	32	Ankle sprain; snowboarding	Acute	Ankle sprain; syndesmosis injury (physical exam, radiologic findings)	+	N/A	N/A	+	N/A	N/A	Evidence of syndesmosis widening
M	57	Ankle sprain; snowboarding	Acute	Syndesmosis tear (physical exam, radiologic findings)	+	±	+	−	−	N/A	Unremarkable
M	58	Ankle sprain; hiking	Acute	Distal lateral malleolar fracture; lateral/syndesmosis sprains; cystic calcaneus	+	−	+	+	−	N/A	Distal lateral malleolar fracture
M	29	Contact injury	Acute	Maisonneuve fracture; medial/syndesmosis tenderness	+	N/A	N/A	N/A	N/A	N/A	Mildly displaced proximal spiral fibular fracture; medial clear and tibiofibular space widening
F	55	External rotation injury	Acute	Maisonneuve fracture with deltoid and syndesmosis involvement	+	X	X	X	X	X	Fibular fracture; widening medial mortise clear space and some syndesmosis widening
M	42	External rotation injury; mountain biking	Acute	Maisonneuve fracture and ankle dislocation	X	X	X	X	X	X	Increased medial and mortise space; posterior tibial avulsion; non-displaced proximal fibular fracture
M	23	Ankle sprain; weight training	Acute	Significant syndesmosis injury; AITFL tear (MRI findings)	+	−	−	−	+	−	Stress X-rays; consistent with physical exam findings
M	21	External rotation injury; baseball	Acute	Fibular fracture; deltoid and syndesmosis injury (MRI findings)	+	N/A	N/A	N/A	N/A	N/A	Oblique displaced (3 mm) distal fibular fracture; no medial clear space or syndesmosis widening
M	18	Inversion ankle sprain; lacrosse	Acute	Syndesmosis injury (radiologic findings)	+	N/A	−	−	N/A	N/A	Stress X-rays; medial widening, increased tibiofibular clear space
M	19	Plantar flexion inversion ankle sprain; football	Chronic	Chronic syndesmosis injury with instability (MRI findings)	+	N/A	+	N/A	−	−	Unremarkable
M	33	Backwards fall	Acute	Distal fibular fracture; deltoid injury; syndesmosis tear (MRI findings)	+	−	−	N/A	−	−	Minimally displaced lateral malleolar fracture
M	24	Inversion ankle sprain; skiing	Acute	Chronic syndesmosis injury with instability (MRI findings)	+	+	+	+	−	−	Unremarkable

Table 1 continued

M/F	Age	Injury mechanism	Acute/chronic	Indication(s) for surgery	Physical exam					Radiographs
					P/T	CT	ER	SQ	AD	TT	
F	47	Ankle sprain; high heels	Chronic	Syndesmosis instability; anterior syndesmosis tear (MRI findings)	+	+	N/A	N/A	–	–	Unremarkable
M	18	Ankle sprain; skiing	Acute	Syndesmosis tear (MRI findings)	+	+	N/A	N/A	–	–	Unremarkable
F	34	Ankle sprain; fall	Acute	Bi-malleolar fracture; distal fibular fracture; deltoid and syndesmosis tear (MRI findings)	+	N/A	N/A	N/A	–	–	Oblique distal fibular fracture; talar impaction; medial widening
M	22	Ski race crash	Acute	Syndesmosis injury (MRI)	N/A	N/A	N/A	N/A	N/A	N/A	Obtained while in Ski boot; no evidence of fracture

P/T palpation/tenderness, *CT* Cotton test, *ER* external rotation test, *SQ* squeeze test, *AD* anterior drawer test, *TT* talar tilt test, + positive, – negative, ± equivocal, *N/A* not reported/performed, *X* exam limited by pain/fracture

pathology. The asymptomatic volunteer scans were used to characterize the normal syndesmosis appearance.

Arthroscopic data

Due to the standard of care, the surgeon was not blinded to the results of MRI. All patients underwent arthroscopic surgery with standard anterolateral and anteromedial portals. The AITFL was well visualized through the anteromedial portal and could be evaluated along its entire intra-articular course. The PITFL was well visualized through both portals and could be reliably evaluated for mid-substance tearing. The ITFL was not consistently visualized although its integrity could be assessed secondarily by probing the distal tibiofibular articulation with a small elevator or a standard arthroscopic probe for diastasis or widening. The criteria for determining incompetence of the syndesmosis were frank diastasis or the ability to produce diastasis with surgical instruments as described above. Cartilage surfaces were probed arthroscopically, and defects were documented using a calibrated probe to assess cartilage integrity. The International Cartilage Repair Society (ICRS) grade, size, and anatomic location of the defects were recorded on a standardized form immediately following the procedure. When indicated, syndesmotic instability was treated with two divergently placed suture-button fixation devices consisting of ultra-high molecular weight polyethylene (UHMWPE) and polyester braided suture tensioned and fixated between two metallic cortical surgical buttons (TightRope®, Arthrex Inc., Naples, FL). If concurrent fractures were fixed (other than a Maisonneuve-type proximal fibular fracture), a single suture-button construct was utilized. The AITFL was directly repaired when possible (12/21 cases) with #1 or #0 Vicryl suture. Concomitant injuries and their surgical treatment were also recorded at the time of the operation. The collection and use of all volunteer and patient data were approved by the Vail Valley Medical Center Institutional Review Board (VVMC IRB).

Imaging and statistical analysis

Ten asymptomatic volunteers were evaluated with 3.0-T MRI. The MRI appearance of the normal syndesmosis was described, and the optimal MRI sequencing images and imaging planes for viewing each structure of the syndesmosis were identified.

All pre-operative MRI data and intraoperative data were collected prospectively and retrospectively reviewed in the 21 symptomatic patients. Arthroscopy was considered the diagnostic gold standard [23, 39, 40]. Structures not otherwise described in reports were deemed normal or intact. Sensitivity, specificity, positive predictive values (PPV), negative predictive values (NPV), and accuracy of MRI

Table 2 Parameters of the imaging sequences used in the study

Sequence	PD TSE cor	T2W TSE ax	PD TSE sag	PD TSE FS sag	PD TSE FS ax	PD TSE FS cor
Repetition time (ms)	4,340	3,970	2,620	2,570	3,730	4,660
Echo time (ms)	36	111	35	43	43	43
Field of view (mm)	120	120	120	120	120	120
Matrix	384 × 288	320 × 256	384 × 288	320 × 256	320 × 256	320 × 256
Voxel size (mm)	0.4 × 0.35 × 3.0	0.5 × 0.4 × 3.0	0.4 × 0.3 × 3.0	0.5 × 0.4 × 3.0	0.5 × 0.4 × 3.0	0.5 × 0.4 × 3.0
Slice thickness (%)	3	3	3	3	3	3
Distance factor (%)	10 %	20 %	10 %	10 %	20 %	10 %
Number of slices	40	32	23	23	32	30
Echo trains/slice	36	13	64	32	16	16
Turbo factor	8	21	9	8	8	8
Examination time	2:42	1:53	2:52	2:51	2:08	2:40

MR parameters for quantitative and morphological imaging

PD TSE Proton Density Turbo Spin Echo, *Cor* coronal, *T2W TSE* T2 Weighted Turbo Spin Echo, *Ax* axial, *Sag* sagittal, *PD TSE FS* Proton Density Turbo Spin Echo Fat Suppressed

Table 3 Individual syndesmotic structures and optimal MRI sequence(s)

Structure	MRI sequence(s)[a]
AITFL	Axial (PD TSE FS, T2W)
PITFL	Axial (PD TSE FS, T2W)
ITFL	Axial (PD TSE FS, T2W)
Synovial recess	Coronal (PD TSE FS, PD TSE)
	Sagittal (PD TSE FS, PD TSE)
Tibial cartilage	Coronal (PD TSE FS, PD TSE)
Fibular cartilage	Coronal (PD TSE FS, PD TSE)
Talar cartilage	Coronal (PD TSE FS, PD TSE)
	Sagittal (PD TSE FS, PD TSE)

AITFL anterior inferior tibiofibular ligament, *PITFL* posterior inferior tibiofibular ligament, *ITFL* interosseous tibiofibular ligament

[a] Sequence(s) with best visualization of individually specified structures; PD TSE FS, Proton Density Turbo Spin Echo Fat Suppressed; T2W, T2 weighted; PD TSE, Proton Density Turbo Spin Echo

were calculated for the diagnoses of syndesmotic ligament tears, synovial recess pathology, and articular cartilage defects. Concurrent injuries to other ankle structures were recorded during analysis and reported.

Results

Asymptomatic cohort

The optimal MRI sequence and imaging plane to evaluate each syndesmotic structure are presented in Table 3. Magnetic resonance imaging demonstrated the asymptomatic anatomy at 3.0-T for all syndesmotic structures of interest in the asymptomatic cohort and can be appreciated in Figs. 1, 2 and 3. Because the asymptomatic cohort did not undergo arthroscopy, diagnostic accuracy data could not be calculated.

Anterior inferior tibiofibular ligament (AITFL)

In the asymptomatic cohort, the AITFL was trapezoidal in shape, coursing distally and laterally from its tibial origin at the anterolateral (Tillaux-Chaput) tubercle to its insertion on the anteromedial (Wagstaffe) tubercle of the fibula. In the patient cohort, the AITFL was the most commonly injured of the syndesmotic ligaments (Table 4; Fig. 4). Tears of the AITFL were diagnosed with the greatest sensitivity and PPV of any syndesmotic ligament disruption with values of 87.5 and 100 %, respectively (Table 5).

Posterior inferior tibiofibular ligament (PITFL)

The trapezoidal PITFL was composed of both the superficial and deep transverse constituents [1, 9]. The superficial portion originated from the posterolateral (Volkmann) tubercle of the tibia, mirroring the AITFL, coursing distally and laterally to its attachment on the posterior aspect of the fibula. In the axial plane, the fibular insertion of the superficial PITFL was medial to the course of the peroneus longus and brevis tendons along the posterior aspect of the fibula. The deep portion of the PITFL, also referred to as the inferior transverse tibiofibular ligament, originated further medially along the tibial plafond and inserted on the fibula anterior and distal to the superficial fibres [1, 9].

No complete tears of the PITFL were observed arthroscopically (Table 4; Fig. 4). Pre-operative MRI diagnosed one false-positive PITFL tear. Incomplete and/or non-displaced posterior malleolus/tibial avulsion of the PITFL

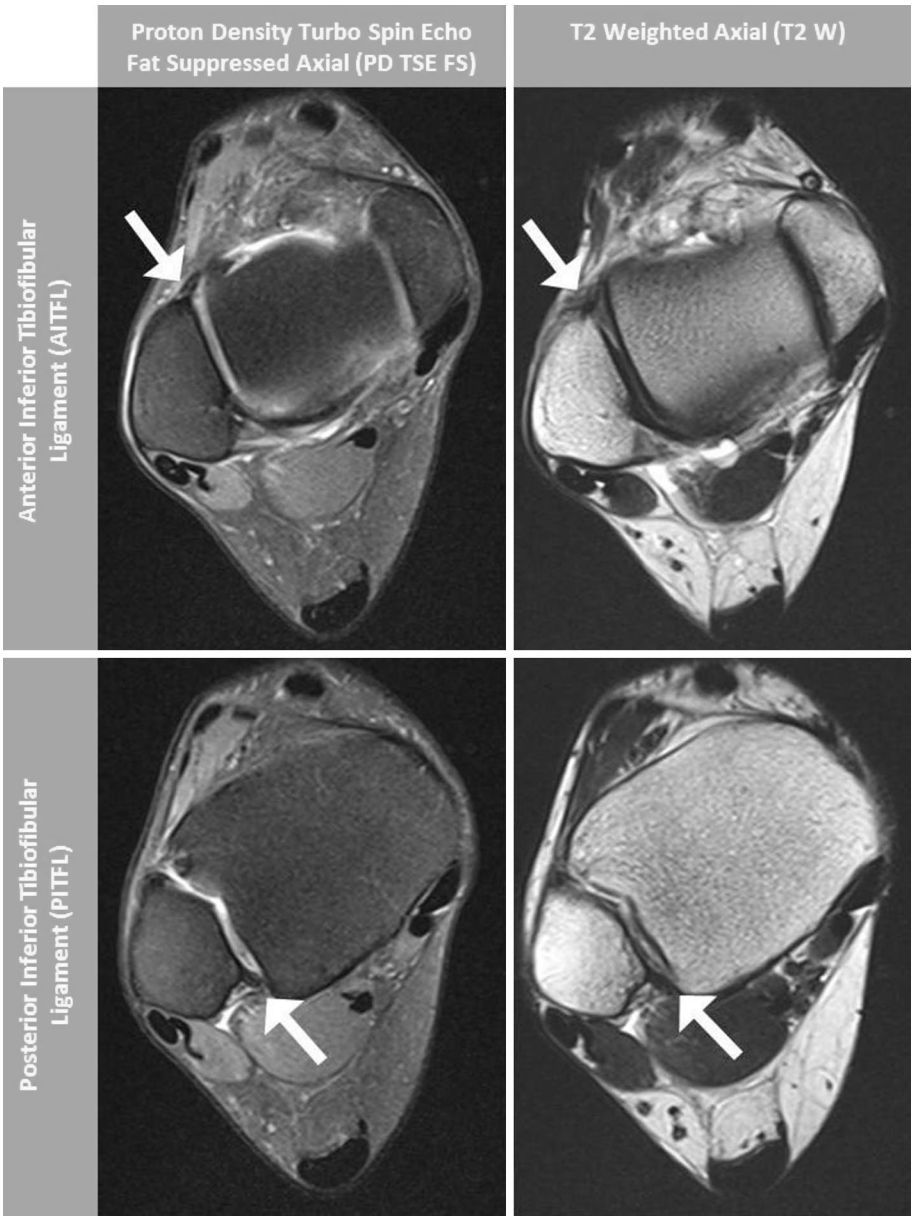

Fig. 1 The MRI appearance of the anterior inferior tibiofibular ligament (AITFL, *top*) and posterior inferior tibiofibular ligament (PITFL, *bottom*) on Proton Density Turbo Spin Echo Fat Suppressed (PD TSE FS, *left*) and T2 weighted (T2W, *right*) axial sequences of a left ankle. *Arrows* indicate the location of the structure of interest

was also noted. Quantitative descriptors demonstrated the ability of MRI to distinguish between ligament ruptures and inflammation with a specificity of 95.2 % and NPV of 100 % for PITFL tears (Table 5). Additionally, due to its frequently observed intact state, it often served as a reproducible reference for other syndesmotic structures.

Interosseous tibiofibular ligament (ITFL)

The ITFL presented as a pyramidal fibrous network with its base beginning approximately 1–2 cm above the tibial plafond at the superior border of the synovial recess. It then narrowed in a pyramidal fashion as it filled the *incisura fibularis tibiae* (fibular notch) proximally, terminating as it transitioned into the distal interosseous membrane.

Interosseous ligament pathology was a relatively common finding on MRI and during arthroscopy (Table 4; Fig. 4). Tears were recognized with relatively good diagnostic sensitivity (66.7 %), which was only exceeded by the sensitivity of AITFL tears for ligament pathology (Table 5).

Synovial recess

The synovial recess originated at the tibial plafond and extended proximally to the distal margin of the ITFL (Fig. 2). Along the anterior border of the syndesmosis, the cartilage-covered facets of both the tibia and fibula were best visualized in the coronal sequences (Table 3; Fig. 3). The tibial and fibular articulating surfaces (contact zones) were confined to approximately the anterior quarter of the

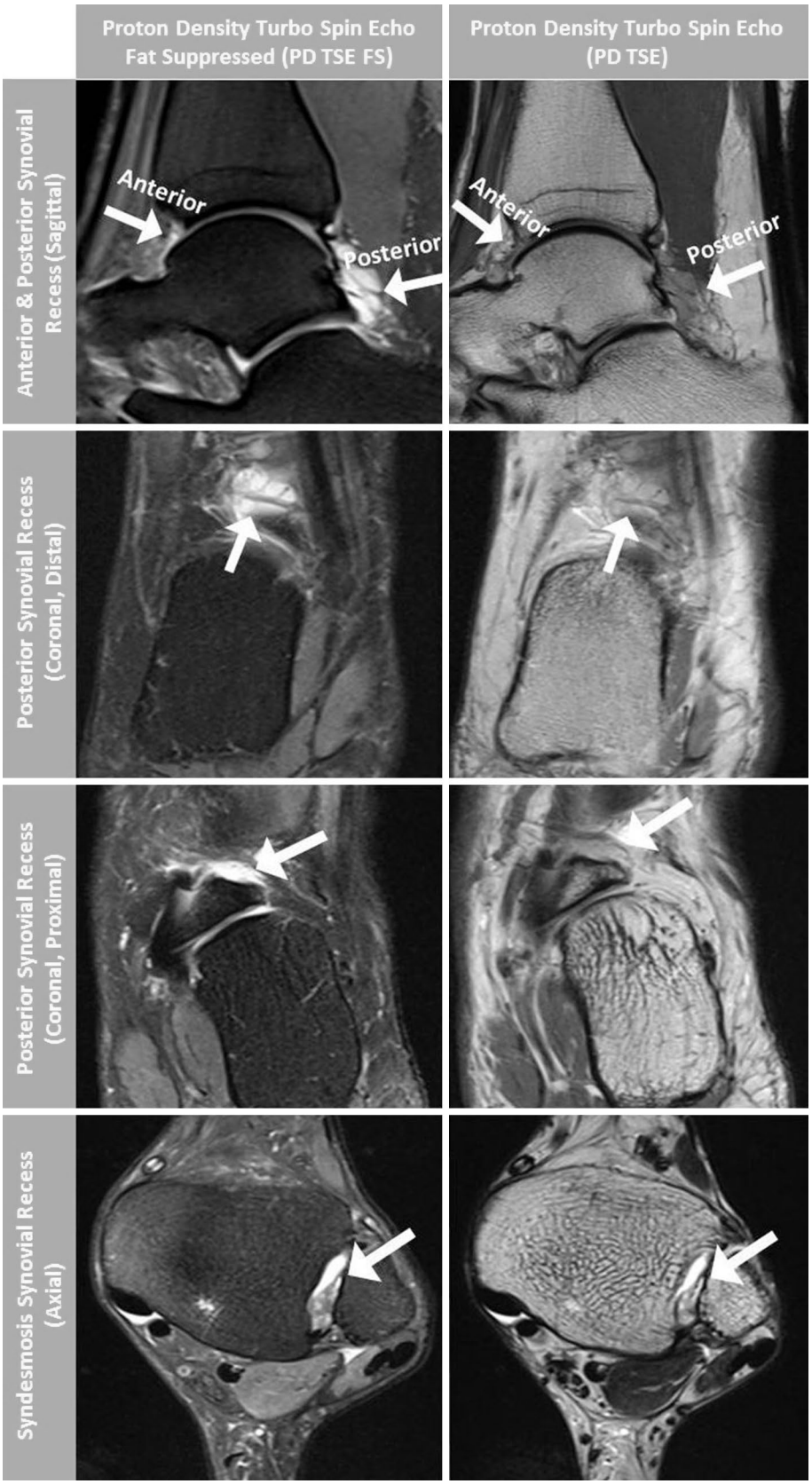

Fig. 2 The MRI appearance of the asymptomatic synovial recess in a right ankle (mild signal increase). Synovial fluid was visible on Proton Density Turbo Spin Echo Fat Suppressed (PD TSE FS, *left*) and Proton Density Turbo Spin Echo (PD TSE, *right*) sequences in sagittal, coronal, and axial (*top to bottom*) planes. *Arrows* indicate areas of interest

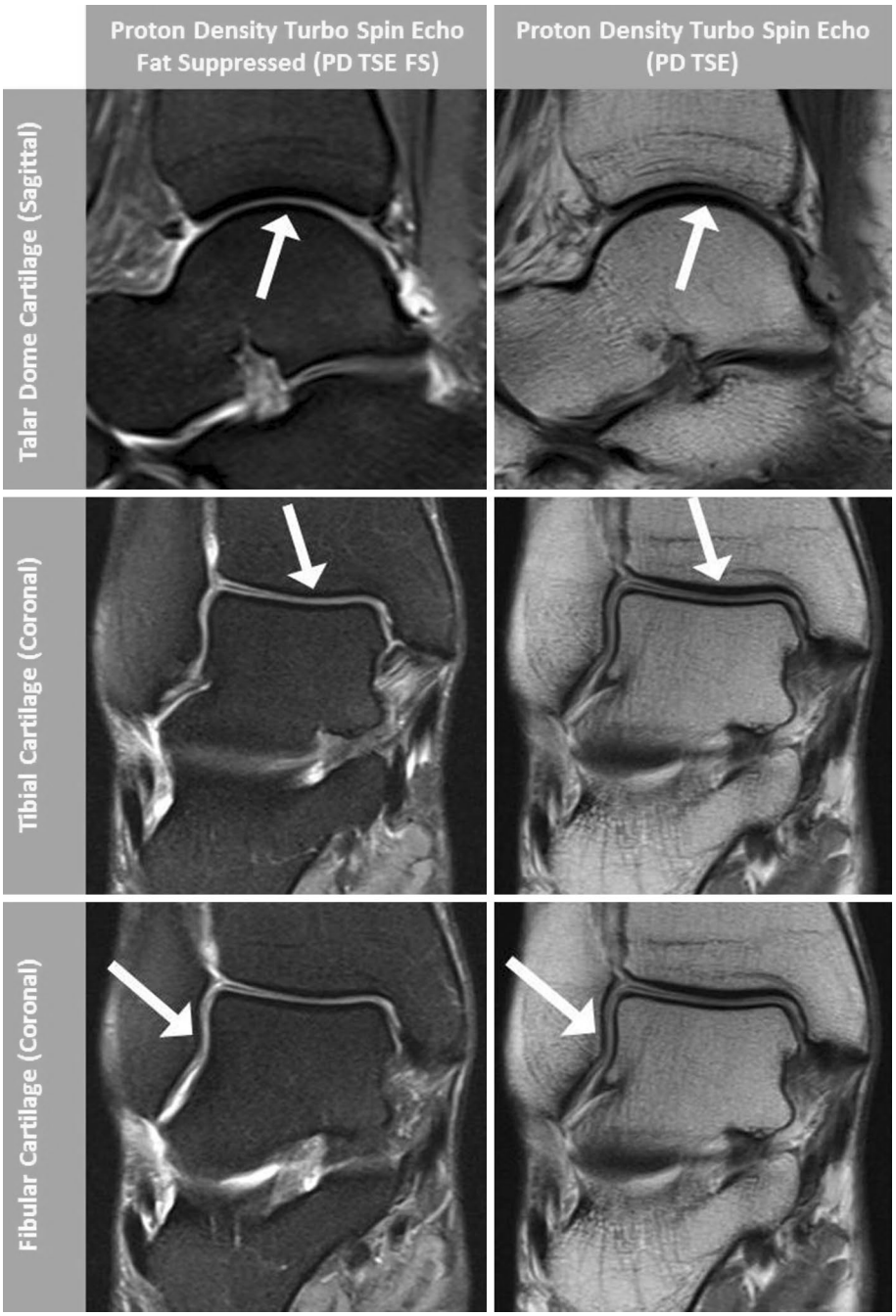

Fig. 3 The MRI appearance of articular cartilage surfaces of a right ankle on Proton Density Turbo Spin Echo Fat Suppressed (PD TSE FS, *left*) and Proton Density Turbo Spin Echo (PD TSE, *right*) sequences. Tibial (*middle*) and fibular (*bottom*) cartilage surfaces were visualized in the coronal sequence, while talar dome cartilage (*top*) was viewed in the sagittal plane. *Arrows* indicate cartilage plates of interest

synovial recess which was consistent with previous anatomic reports [1, 9].

Within the injured patient population, prominent synovial recess scarring and synovitis were readily apparent on both MRI and arthroscopic examination (Fig. 4; Table 4). Diffuse synovitis was frequently used as a general descriptor of the joint both on MRI and arthroscopy resulting in a high sensitivity (82.4 %) but a lack of diagnostic specificity (0.0 %) (Table 5).

Articular cartilage

The articular cartilage surfaces of the tibia, fibula, and talus were best observed on the PD TSE FS and PD TSE sequences of the coronal and sagittal images (Fig. 3; Table 3). The coronal and sagittal planes allowed for optimal diagnosis of a wide range of osteochondral injuries in patients with syndesmotic injuries (Figs. 5, 6, 7; Tables 5, 6). The majority of patients (61.9 %) had at least one tibial

Table 4 Correlation of normal and injured MRI appearance versus surgical confirmation in 21 ankles with syndesmotic injuries

Structure[a]	MRI appearance			Surgical findings[c]	
	Normal	Sprained/scarred	Torn	Intact	Torn
AITFL	0	7	14	5	16
PITFL	1	19	1	21	0
ITFL	9	6	6	15	6
	Normal	Synovitis		Normal	Synovitis
Synovial recess	3	18	–	4	17
	Normal	Thinning/fissuring	Focal lesion	Normal	Lesion
Tibial cartilage	11	9	1	13	8
Fibular cartilage	–	–	–	–	–
Talar cartilage	13	7	1	10	11

AITFL anterior inferior tibiofibular ligament, *PITFL* posterior inferior tibiofibular ligament, *ITFL* interosseous tibiofibular ligament

[a] Structures not otherwise described as injured in arthroscopic operation reports were deemed intact/uninjured; sprains, scarring, and synovitis were deemed "intact"; –, not reported/applicable

or talar osteochondral defect, while 28.6 % had arthroscopic confirmation of injuries to both tibial and talar articular cartilage surfaces (Table 4). False-negative diagnoses of cartilage defects (3 Tibial, 5 Talar) on MRI were minor (grade 1 and 2 chondromalacia graded arthroscopically).

Injuries to the syndesmosis and concomitant pathology

The AITFL was found to be torn in surgery in 16 (76.2 %) patients, and it was the only torn syndesmotic ligament in 10 (47.6 %) cases. Six injuries involved both AITFL and interosseous ligament/membrane tears, while no complete syndesmosis injuries were observed. In the patient cohort, syndesmotic injuries were frequently accompanied by other ankle pathology. Isolated injuries to the syndesmosis were rarely reported either pre-operatively on MRI or intra-operatively at the time of arthroscopy (23.8 %). Concurrent fractures, ligamentous injury, tendon tears, osteochondral lesions, interosseous membrane tears, and synovitis were frequently observed at the time of surgery (Table 6).

Discussion

The most important finding of this study was the ability of high-field MRI to visualize injuries to individual syndesmotic structures and identify frequently observed ligament tears with excellent diagnostic accuracy. Furthermore, PPV and NPV for the AITFL (100, 71.4 %), PITFL (0.0 %, 100 %), and ITFL (66.7, 86.7 %) demonstrated the superior diagnostic power of high-field MRI compared with other current clinical methods of injury detection.

In the asymptomatic population, the AITFL consistently correlated with its anatomic position and descriptions within the literature [1, 9]. Derangements including sprains and tears were readily apparent on MRI. Tears of the AITFL were diagnosed with the greatest sensitivity, specificity, and PPV in comparison with the other syndesmotic structures. These findings are encouraging based on incidence reports demonstrating that the AITFL is the most often injured of the syndesmotic ligaments [13, 27, 40]. The frequency of AITFL pathology is often attributed to its strength relative to other syndesmotic structures and the commonly hypothesized coupled dorsiflexion and external rotation injury mechanism [10, 19, 28, 32]. Given the frequency of AITFL injury in comparison to other structures, improved characterization of the AITFL via MR imaging is clinically relevant and may help improve patient outcomes by guiding treatment. Similarly, the MRI appearance of the PITFL corresponded with previous anatomic characterizations including the superficial and deep origins and insertions. In the injured population, no complete ruptures were observed. Although the absence of complete PITFL ruptures prevented the calculation of sensitivity data, specificity and NPV values demonstrated the ability of 3.0-T MRI to repeatedly distinguish between sprains and complete mid-substance tears.

The accurate diagnosis and subsequent treatment of syndesmotic injuries are important to prevent the development of chronic ankle pain, instability, altered joint kinematics, and subsequent chondral injury that can result from an undiagnosed injury and inadequate course of treatment [30]. Ramsey et al. [31] demonstrated that tibiotalar contact areas are reduced by as much 42 % with 1 mm lateral

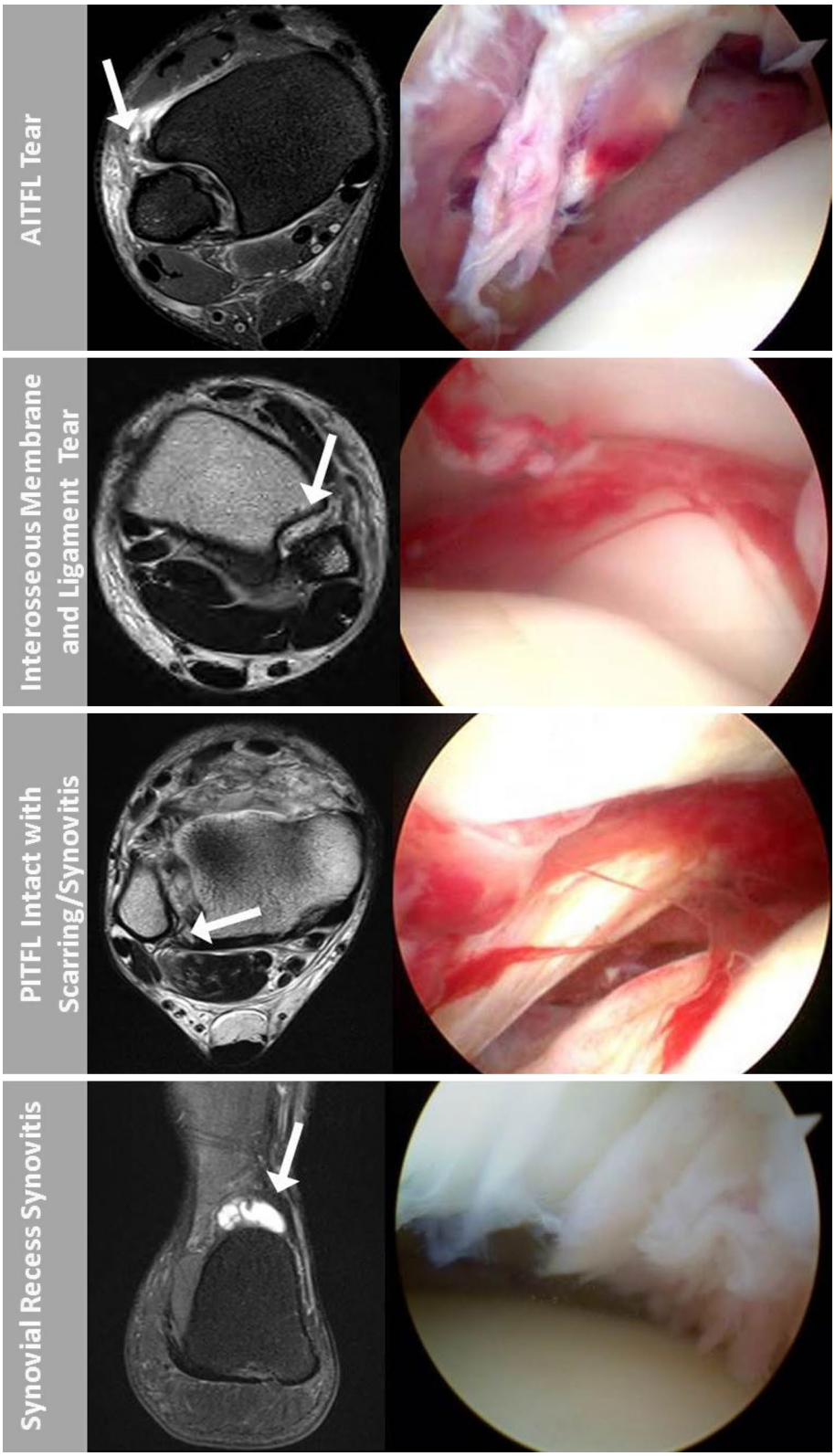

Fig. 4 The MRI and arthroscopic correlation of injuries to individual syndesmotic structures. *Top to bottom* anterior inferior tibiofibular ligament (AITFL) tear in a left ankle (Proton Density Turbo Spin Echo Fat Suppressed axial, anteromedial portal); interosseous tibiofibular ligament (ITFL) and membrane tear in a right ankle (T2 weighted axial, anteromedial portal); posterior inferior tibiofibular ligament (PITFL) sprain in a left ankle (T2 weighted axial, anterolateral portal); synovial recess scarring and synovitis in a left ankle (Proton Density Turbo Spin Echo Fat Suppressed coronal, anteromedial portal)

displacement that can result from syndesmosis tears and instability. Over time, such alterations in joint kinematics can result in poor clinical outcomes and post-traumatic arthritic chondral changes [30]. In this patient cohort, high-field MRI also served in the detection of acute chondral and impaction injuries not readily seen on standard radiographs. In this

Table 5 Diagnostic accuracy of MRI compared with arthroscopic findings in 21 ankles with syndesmotic injuries

Structure	Sensitivity	Specificity	PPV	NPV	Accuracy
AITFL	87.5 %	100.0 %	100.0 %	71.4 %	90.5 %
PITFL	N/A	95.2 %	0.0 %	100.0 %	95.2 %
ITFL	66.7 %	86.7 %	66.7 %	86.7 %	81.0 %
Synovial recess	82.4 %	0.0 %	77.8 %	0.0 %	66.7 %
Tibial Cartilage	62.5 %	61.5 %	50.0 %	72.7 %	61.9 %
Fibular Cartilage	–	–	–	–	–
Talar Cartilage	54.5 %	80.0 %	75.0 %	61.5 %	66.7 %

AITFL anterior inferior tibiofibular ligament, *PITFL* posterior inferior tibiofibular ligament, *ITFL* interosseous tibiofibular ligament, *PPV* positive predictive value, *NPV* negative predictive value, *N/A* could not be calculated due to a lack of surgically confirmed PITFL injuries, – not reported/applicable

diagnostic accuracy study, the MRI characterization of the syndesmosis in both asymptomatic volunteers and injured patients demonstrated the ability of MRI to visualize individual syndesmotic structures. Furthermore, the data presented confirmed the ability of high-field MRI to diagnose the most common syndesmotic injuries with a high degree of accuracy when comparing to the gold standard of arthroscopy.

Compared with other techniques including physical examination, radiography (both standard and stress), and fluoroscopy under anaesthesia, MRI provided a reproducible and non-invasive diagnostic technique that exceeded the currently reported accuracies of other diagnostic techniques [4, 8, 13, 23, 26, 29, 33–35, 37, 42]. Clinical examination alone lacks sufficient sensitivity and specificity as documented by Beumer et al. [3]. Several specific clinical examinations such as the anterior drawer, squeeze test, Cotton test, fibular translation, external rotation, and dorsiflexion have demonstrated diagnostic accuracies ranging from 33.3 to 61.9 % [3, 35, 37]. Similar studies have since corroborated these conclusions. In a cross-sectional diagnostic accuracy study, Sman et al. [35, 37] demonstrated that no single test is sufficiently accurate for the diagnosis of syndesmosis injury. Similar doubts have been cast regarding accuracy of radiographic evaluation in both cadaveric models and clinical investigations [4, 23, 26, 29]. Pneumaticos et al. [29] demonstrated that many radiographic parameters used to assess syndesmosis injuries, including tibiofibular overlap and medial clear space, vary significantly depending on the rotational orientation of the extremity. In a cadaveric study, Beumer et al. [4] subsequently concluded that external rotation stress radiography is unreliable for the diagnosis of syndesmosis instability because significant increases in external rotation were only observed after the transection of multiple ligaments (e.g. ATIFL + PITFL). Clinically, research has demonstrated that stress radiography is able to detect less than half of the instability confirmed arthroscopically [23]. Moreover, stress radiography often requires some level of patient anesthetization, thus making it less feasible in routine clinical practice.

These trends of difficulty and inconclusive clinical diagnosis were apparent in the current patient cohort. Many patients presenting with negative or equivocal clinical examination and radiographic results were later found to have syndesmotic injuries requiring surgical fixation at the time of arthroscopy. In such cases, surgical treatment was often indicated by MRI findings. Therefore, the authors contend that 3.0-T MRI offers a more desirable and fruitful technique for diagnosing syndesmotic injuries, in addition to related ligamentous, osseous, and chondral

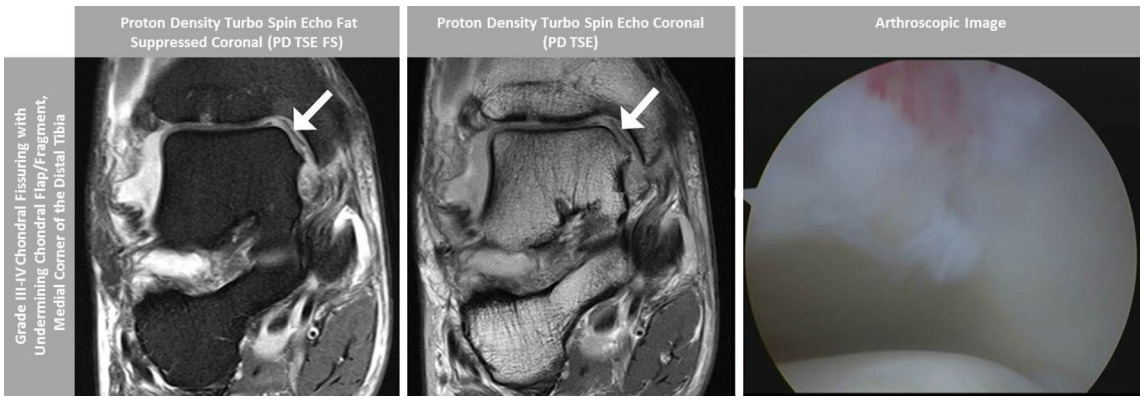

Fig. 5 The MRI and arthroscopic correlation of a Grade III–IV chondral injury in a right ankle on the distal medial tibia as viewed on the Proton Density Turbo Spin Echo Fat Suppressed (PD TSE FS, *left*) and Proton Density Turbo Spin Echo (PD TSE, *middle*) coronal sequences and through the standard anterolateral arthroscopic portal (*right*)

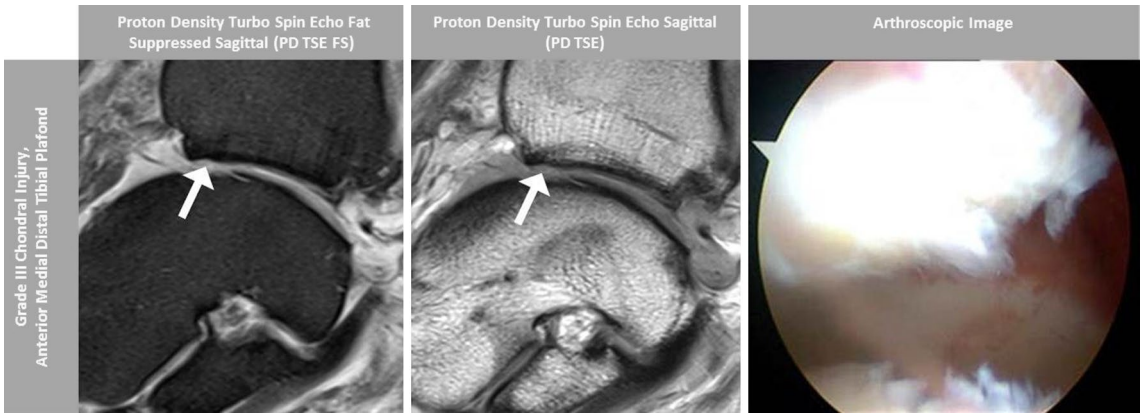

Fig. 6 The MRI and arthroscopic correlation of a Grade III chondral injury in a right ankle of the anterior medial distal tibial plafond as viewed on the Proton Density Turbo Spin Echo Fat Suppressed (PD TSE FS, *left*) and Proton Density Turbo Spin Echo (PD TSE, *middle*) sagittal sequences and through the standard anteromedial arthroscopic portal (*right*)

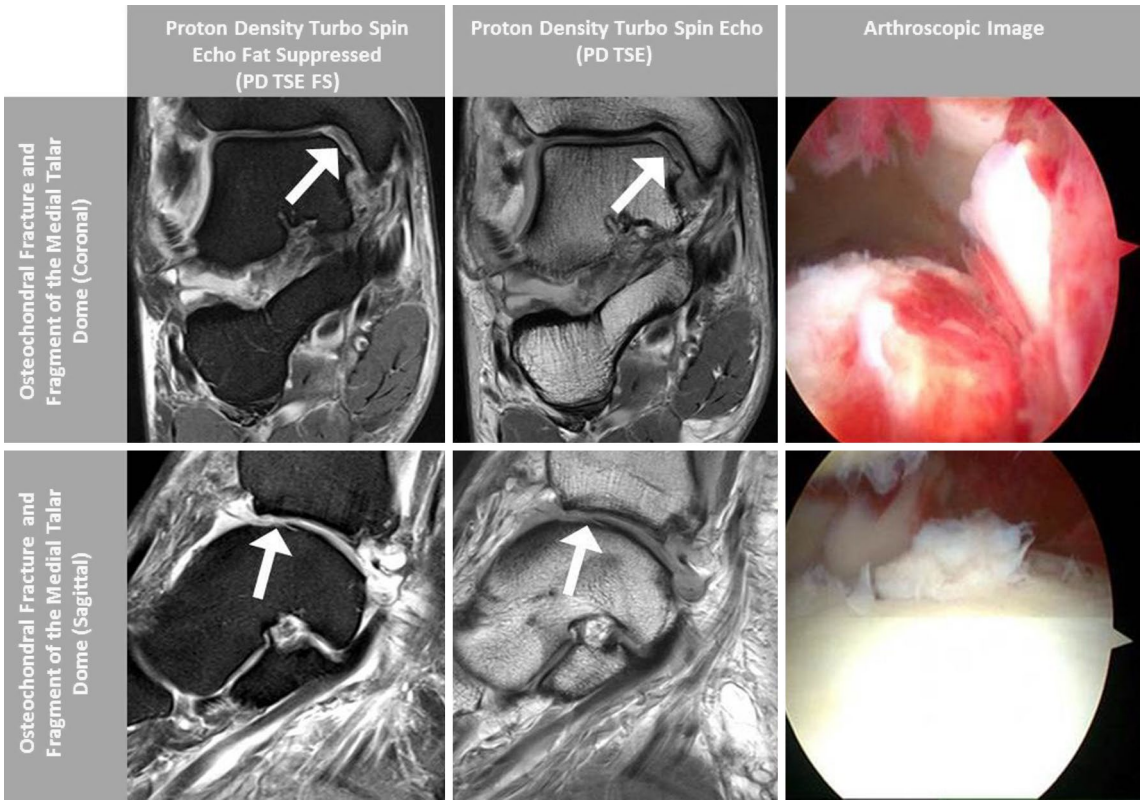

Fig. 7 The MRI and arthroscopic correlation of a talar osteochondral fracture and fragment in a right ankle as viewed on the Proton Density Turbo Spin Echo Fat Suppressed (PD TSE FS, *left*) and Proton Density Turbo Spin Echo (PD TSE, *middle*) coronal (*top*) and sagittal (*bottom*) sequences. Arthroscopic images (*right*) were taken from standard anteromedial (*top*) and anterolateral (*bottom*) portals

injuries. High-field ankle MRI is an exceedingly useful, non-invasive technique that provides superior accuracy and improved patient comfort in comparison with the other currently available assessment modalities while eliminating patient exposure to ionizing radiation from procedures including stress radiography and fluoroscopy.

The authors acknowledge the limitations of the present study. Foremost, the study involved a retrospective recall

Table 6 Frequency of surgically diagnosed concomitant ankle pathology

Concomitant injury	Frequency
Fracture	**12**
Maisonneuve fracture	3
Proximal fibula	3
Distal fibula	2
Lateral malleolar	1
Medial malleolar	1
Bi-malleolar	1
Tri-malleolar	1
Additional ligamentous pathology	
Deltoid injury	7
Tear	4
Sprain	3
Tendon pathology	
Tear	
Peroneus brevis	1
Tenosynovitis	
Peroneus brevis	1
Peroneus longus	1
Interosseous membrane tear	**3**
Osteochondral pathology	
Tibia	
Fracture (distal tibia)	1
Grade 3/4	1
Grade 1/2	6
Talus	
Fracture (talar dome)	1
Grade 3/4	0
Grade 1/2	10
Synovitis	**17**

of prospectively collected ankle MRI and arthroscopic data which did not allow for surgeon blinding to MRI findings at the time of arthroscopy. Such blinding would have changed the standard of care in these patients and therefore blinding could not be implemented. There is the potential that this inherent limitation could have influenced the findings of arthroscopy, and the results of the present study must be interpreted accordingly. The authors also acknowledge the potential limitations of the present patient sample. The age range, although broad, is consistent with previous investigations [23, 27, 40]. The sample size is relatively small due to a limited number of eligible cases; however, the patient sample is comparable to similar previous diagnostic studies [13, 17, 42, 43]. Finally, the authors recognize the predominance of male patients; however, previous studies with varying gender proportions have not documented any discrepancies in MRI or arthroscopic diagnostic parameters between genders. Therefore, the authors do not believe that this significantly influenced the results and interpretation of the presented patient sample.

Conclusions

This high-field MRI analysis refined the visualization of individual syndesmosis structures and identified the optimal ankle MRI image plane/sequence(s) for characterizing both the normal and injured structures of the ankle syndesmosis. The results demonstrated the accuracy and reproducibility of MRI in diagnosing common syndesmotic injuries with an excellent degree of sensitivity, specificity, PPV, and NPV. High-field ankle MRI at 3.0-T can therefore be utilized to augment equivocal physical examination findings and inconclusive radiographic results in the clinical diagnosis and evaluation of AITFL, PITFL, and ITFL tears, and associated chondral injuries and synovial pathology.

References

1. Bartonicek J (2003) Anatomy of the tibiofibular syndesmosis and its clinical relevance. Surg Radiol Anat 25(5–6):379–386
2. Bauer JS, Banerjee S, Henning TD, Krug R, Majumdar S, Link TM (2007) Fast high-spatial-resolution MRI of the ankle with parallel imaging using GRAPPA at 3 T. AJR Am J Roentgenol 189(1):240–245
3. Beumer A, Swierstra BA, Mulder PG (2002) Clinical diagnosis of syndesmotic instability evaluation of stress tests behind the curtains. Acta Orthop Scand 73(6):667–669
4. Beumer A, Valstar ER, Garling EH, van Leeuwen WJ, Sikma W, Niesing R, Ranstam J, Swierstra BA (2003) External rotation stress imaging in syndesmotic injuries of the ankle: comparison of lateral radiography and radiostereometry in a cadaveric model. Acta Orthop Scand 74(2):201–205
5. Beumer A, van Hemert WL, Niesing R, Entius CA, Ginai AZ, Mulder PG, Swierstra BA (2004) Radiographic measurement of the distal tibiofibular syndesmosis has limited use. Clin Orthop Relat Res 423:227–234
6. Brown KW, Morrison WB, Schweitzer ME, Parellada JA, Nothnagel H (2004) MRI findings associated with distal tibiofibular syndesmosis injury. AJR Am J Roentgenol 182(1):131–136
7. Cedell CA (1975) Ankle lesions. Acta Orthop Scand 46(3):425–445
8. César de César PC, Avila EM, de Abreu MR (2011) Comparison of magnetic resonance imaging to physical examination for syndesmotic injury after lateral ankle sprain. Foot Ankle Int 32(12):1110–1114
9. Ebraheim NA, Taser F, Shafiq Q, Yeasting RA (2006) Anatomical evaluation and clinical importance of the tibiofibular syndesmosis ligaments. Surg Radiol Anat 28(2):142–149
10. Fritschy D (1989) An unusual ankle injury in top skiers. Am J Sports Med 17(2):282–285
11. Gerber JP, Williams GN, Scoville CR, Arciero RA, Taylor DC (1998) Persistent disability associated with ankle sprains: a prospective examination of an athletic population. Foot Ankle Int 19(10):653–660
12. Griffith JF, Lau DT, Yeung DK, Wong MW (2012) High-resolution MR imaging of talar osteochondral lesions with new classification. Skeletal Radiol 41(4):387–399

13. Han SH, Lee JW, Kim S, Suh JS, Choi YR (2007) Chronic tibiofibular syndesmosis injury: the diagnostic efficiency of magnetic resonance imaging and comparative analysis of operative treatment. Foot Ankle Int 28(3):336–342
14. Harper MC, Keller TS (1989) A radiographic evaluation of the tibiofibular syndesmosis. Foot Ankle 10(3):156–160
15. Hermans JJ, Beumer A, de Jong TA, Kleinrensink GJ (2010) Anatomy of the distal tibiofibular syndesmosis in adults: a pictorial essay with multimodality approach. J Anat 217(6):633–645
16. Hermans JJ, Beumer A, Hop WC, Moonen AF, Ginai AZ (2012) Tibiofibular syndesmosis in acute ankle fractures—additional value of an oblique MR image plane. Skelet Radiol 41(2):193–202
17. Hermans JJ, Ginai AZ, Wentink N, Hop WC, Beumer A (2011) The additional value of an oblique image plane for MRI of the anterior and posterior distal tibiofibular syndesmosis. Skelet Radiol 40(1):75–83
18. Hermans JJ, Wentink N, Beumer A, Hop WC, Heijiboer MP, Moonen AF, Ginai AZ (2012) Correlation between radiological assessment of acute ankle fractures and syndesmotic injury on MRI. Skelet Radiol 41(7):787–801
19. Hopkinson WJ, Pierre PS, Ryan JB, Wheeler JH (1990) Syndesmosis sprains of the ankle. Foot Ankle 10(6):325–330
20. Hunt KJ (2013) Syndesmosis injuries. Curr Rev Musculoskelet Med 6(4):304–312
21. Hunt KJ, George E, Harris AH, Dragoo JL (2013) Epidemiology of syndesmosis injuries in intercollegiate football: incidence and risk factors from National Collegiate Athletic Association injury surveillance system data 2004–2005 to 2008–2009. Clin J Sport Med 23(4):278–282
22. Kim S, Huh YM, Song HT, Lee SA, Lee JW, Lee JE, Chung IH, Suh JS (2007) Chronic tibiofibular syndesmosis injury of the ankle: evaluation with contrast-enhanced fat-suppressed 3D fast spoiled gradient-recalled acquisition in the steady state MR imaging. Radiology 242(1):225–235
23. Lui TH, Ip K, Chow HT (2005) Comparison of radiologic and arthroscopic diagnoses of distal tibiofibular syndesmosis disruption in acute ankle fracture. Arthroscopy 21(11):1370
24. McCollum GA, van den Bekerom MP, Kerkhoffs GM, Calder JD, van Dijk CN (2013) Syndesmosis and deltoid ligament injuries in the athlete. Knee Surg Sports Traumatol Arthrosc 21(6):1328–1337
25. Muhle C, Frank LR, Rand T, Ahn JM, Yeh LR, Trudell D, Haghighi P, Resnick D (1998) Tibiofibular syndesmosis: high resolution MRI using a local gradient coil. J Comput Assist Tomogr 22(6):938–944
26. Nielson JH, Gardner MJ, Peterson MG, Sallis JG, Potter HG, Helfet DL, Lorich DG (2005) Radiographic measurements do not predict syndesmotic injury in ankle fractures: an MRI study. Clin Orthop Relat Res 436:216–221
27. Oae K, Takao M, Naito K, Uchio Y, Kono T, Ishida J, Ochi M (2003) Injury of the tibiofibular syndesmosis: value of MR imaging for diagnosis. Radiology 227(1):155–161
28. Ogilvie-Harris DJ, Reed SC, Hedman TP (1994) Disruption of the ankle syndesmosis: biomechanical study of the ligamentous restraints. Arthroscopy 10(5):558–560
29. Pneumaticos SG, Noble PC, Chatziioannou SN, Trevino SG (2002) The effects of rotation on radiographic evaluation of the tibiofibular syndesmosis. Foot Ankle Int 23(2):107–111
30. Rammelt S, Zwipp H, Grass R (2008) Injuries to the distal tibiofibular syndesmosis: an evidence-based approach to acute and chronic lesions. Foot Ankle Clin 13(4):611–633
31. Ramsey PL, Hamilton W (1976) Changes in tibiotalar area of contact caused by lateral talar shift. J Bone Joint Surg Am 58(3):356–357
32. Rasmussen O (1985) Stability of the ankle joint. Analysis of the function and traumatology of the ankle ligaments. Acta Orthop Scan Suppl 211:1–75
33. Shah AS, Kadakia AR, Tan GJ, Karadsheh MS, Wolter TD, Sabb B (2012) Radiographic evaluation of the normal distal tibiofibular syndesmosis. Foot Ankle Int 33(10):870–876
34. Sikka RS, Fetzer GB, Sugarman E, Wright RW, Fritts H, Boyd JL, Fischer DA (2012) Correlating MRI findings with disability in syndesmotic sprains of NFL players. Foot Ankle Int 33(5):371–378
35. Sman AD, Hiller CE, Rae L, Linklater J, Black DA, Nicholoson LL, Burns J, Refshauge KM (2013) Diagnostic accuracy of clinical tests for ankle syndesmosis injury. Br J Sports Med. doi:10.1136/bjsports-2013-092787
36. Sman AD, Hiller CE, Rae K, Linklater J, Black DA, Refschuage KM (2014) Prognosis of ankle syndesmosis injury. Med Sci Sports Exerc 46(4):671–677
37. Sman AD, Hiller CE, Refshauge KM (2013) Diagnostic accuracy of clinical tests for diagnosis of ankle syndesmosis injury: a systematic review. Br J Sports Med 47(10):620–628
38. Stoffel K, Wysocki D, Baddour E, Nicholls R, Yates P (2009) Comparison of two intraoperative assessment methods for injuries to the ankle syndesmosis. A cadaveric study. J Bone Joint Surg Am 91(11):2646–2652
39. Takao M, Ochi M, Naito K, Iwata A, Kawasaki K, Tobita M, Mivamoto W, Oae K (2001) Arthroscopic diagnosis of tibiofibular syndesmosis disruption. Arthroscopy 17(8):836–843
40. Takao M, Ochi M, Oae K, Naito K, Uchio Y (2003) Diagnosis of a tear of the tibiofibular syndesmosis. The role of arthroscopy of the ankle. J Bone Joint Surg Br 85(3):324–329
41. Van den Bekerom MP (2011) Diagnosing syndesmotic instability in ankle fractures. World J Orthop 2(7):51–56
42. Vincelette P, Laurin CA, Lévesque HP (1972) The footballer's ankle and foot. Can Med Assoc J 107(9):872–874
43. Vogl TJ, Hochmuth K, Diebold T, Lubrich J, Hofmann R, Stöckle U, Söllner O, Bisson S, Südkamp N, Maeurer J, Haas N, Felix R (1997) Magnetic resonance imaging in the diagnosis of acute injured distal tibiofibular syndesmosis. Invest Radiol 32(7):401–409
44. Xenos JS, Hopkinson WJ, Mulligan ME, Olson EJ, Popovic NA (1995) The tibiofibular syndesmosis. Evaluation of the ligamentous structures, methods of fixation, and radiographic assessment. J Bone Joint Surg Am 77(6):847–856
45. Williams GN, Jones MH, Amendola A (2007) Syndesmotic ankle sprains in athletes. Am J Sports Med 35(7):1197–1207
46. Zindrick MR, Hopkins DE, Knight GW (1985) The effects of lateral talar shift upon the biomechanics of the ankle joint. Orthop Trans 9:332–333